Antiferromagnetic Order and Possible Quantum Spin Liquid in Kagome Antiferromagnet $LuCu_3(OH)_6Br_2[Br_x(OH)_{1-x}]$

Zezhong Li(李泽众)[1,2], Lankun Han(韩岚琨)[1,2], Yili Sun(孙毅丽)[1,2], Shanshan Zhang(张珊珊)[1,2], Zhenyuan Zeng(曾振源)[1,2], and Shiliang Li(李世亮)[1,2*]

[1]*Beijing National Laboratory for Condensed Matter Physics, Institute of Physics, Chinese Academy of Sciences, Beijing 100190, China*
[2]*School of Physical Sciences, University of Chinese Academy of Sciences, Beijing 100049, China*

(Received 25 November 2024; accepted manuscript online 24 January 2025)

Recent studies on the kagome lattice $YCu_3(OH)_{6+x}X_{3-x}$ (X = Cl, Br) have provided promising evidence for the existence of Dirac quantum spin liquids. In this study, we synthesized a new compound, $LuCu_3(OH)_6Br_2[Br_x(OH)_{1-x}]$, which has two types of structures with two different space groups, $P\bar{3}m1$ and $R\bar{3}$. The type-I sample with a space group of $P\bar{3}m1$ had undistorted Cu^{2+} kagome planes and orders magnetically below approximately 1.5 K. The type-Ⅱ sample had a larger unit cell with a space group of $R\bar{3}$ and distorted kagome planes. No magnetic ordering was observed, and the low-temperature specific heat behaved like a Dirac quantum spin liquid, including a quadratic temperature dependence at zero field and an additional linear T term under magnetic fields. By comparing the structures with those of $YCu_3(OH)_{6+x}X_{3-x}$ (X = Cl, Br), we show that the quantum spin liquid ground state may have a deep connection with the $J_{\bigcirc}$-J-J' Heisenberg model in the kagome lattice.

DOI: 10.1088/0256-307X/42/2/027504 CSTR: 32039.14.0256-307X.42.2.027504

Two-dimensional kagome Heisenberg antiferromagnet (KHA) systems are very important in the search for quantum spin liquids (QSLs),[1–10] which represent a class of quantum magnetism with anomalously high degrees of entanglement. Theoretical studies show that one of the leading ground states of the QSLs in KHAs is the gapless U(1) Dirac QSL.[11–16] The gapless spinons in a Dirac QSL have a spectrum that can be described by the Dirac function, similar to Dirac cones in the electronic band structures of graphene and topological insulators.[17–19] Recently, the kagome system $YCu^{3+}(OH)_6Br_2[Br_{1-x}(OH)_x]$ (YCu_3-Br) has provided promising evidence for the existence of a Dirac QSL. Its low-temperature specific heat exhibits a T^2 temperature dependence at zero field and an additional linear T term under magnetic fields, which is expected for a U(1) Dirac QSL.[20] Inelastic neutron scattering also exhibits a low-energy conical continuum,[21] which can reproduce the specific-heat results expected of a U(1) Dirac QSL.[11] Notably, a one-ninth magnetization plateau and quantum oscillations at high fields have been observed in this system,[22–25] further suggesting that the YCu_3-Br system is an exciting platform for studying physics in KHAs. However, the Q positions of the low-energy spin excitations deviate from those predicted by the typical KHA model,[7] likely due to the unique structure of this system.

Although the Cu^{2+} ions form perfect kagome planes, there are significant site disorder and randomness in YCu_3-Br. This is because the Br^- ions in the $[CuO_4Br_2]$ octahedra are partially replaced by $(OH)^-$ ions.[26] The polar effect of $(OH)^-$ ions pulls the Y^{3+} ion out of the kagome plane and causes the Cu-O-Cu angles to change alternately,[27] resulting in alternate-bond hexagons (ABHs) with exchange couplings that alternate within the hexagons. The magnetically disordered state has been found to emerge only when the proportion of ABHs is approximately two thirds,[28] suggesting its importance for understanding the origin of the Dirac QSL.

The $Y_3Cu_9(OH)_{19}Cl_8$ (Y_3Cu_9-Cl) system is provides a valuable platform for investigating the role of ABHs. The occupancies of $(OH)^-$ and Cl^- in the $[CuO_4(Cl,O)_2]$ octahedra alternate at a ratio of 1:2, leading to a larger unit cell with the space group $R\bar{3}$. Thus, the detailed structures of the ABHs and unaffected uniform hexagons (UHs) can be studied well because there is no randomness. Both magnetically disordered and AFM-ordered ground states have been previously reported.[29–32] In the AFM samples, the ground state is the $Q = (1/3, 1/3)$ AFM order,[32] which can be described well by the $J_{\bigcirc}$-J-J' Heisenberg model on the kagome lattice.[33] In this model, $J_{\bigcirc}$ represents the nearest exchange coupling within the UHs, and J and J' represent the nearest exchange couplings within the ABHs. This model is related to YCu_3-Br because the Q positions of the low-energy spin excitations in YCu_3-Br and Y_3Cu_9-Cl are identical.[21,32] Also worth noting is that the nuclear superstructure peaks associated with the $R\bar{3}$ space group were also found in YCu_3-Br.[26] This clearly suggests that the ABHs in YCu_3-Br cannot be randomly distributed. An important question then arises: Does the

*Corresponding author. Email: slli@iphy.ac.cn
© 2025 Chinese Physical Society and IOP Publishing Ltd. All rights, including for text and data mining, AI training, and similar technologies, are reserved.

$J_{\bigcirc}$-J-J' model alone produce the Dirac QSL, as indicated by the classical spin-liquid regime,[33] or must some kind of randomness be included in this model?

In this study, we replaced the yttrium in YCu_3-Br with lutetium ($LuCu_3$-Br), resulting in two types of samples with different structures. One has a kagome structure with space group $P\bar{3}m1$, which is the same as YCu_3-Br, but shows an AFM order below approximately 1.5 K. The other has distorted kagome lattice with space group $R\bar{3}$ and exhibits Dirac QSL behaviors. These results suggest that a Dirac QSL can emerge in the $R\bar{3}$ structure and is associated with the $J_{\bigcirc}$-J-J' model. Moreover, because the exchange energies are smaller, the $LuCu_3$-Br system may provide more opportunities for studying high-field physics.

Single crystals of $LuCu_3$-Br were synthesized using a hydrothermal method, following a procedure analogous to that employed for YCu_3-Br.[20,26,28] $Cu(NO_3)_2{\cdot}3H_2O$ (2.5 mmol), $Lu(NO_3)_3{\cdot}6H_2O$ (5 mmol), and KBr (15 mmol) were mixed with 1.2 mL of deionized water in a 25-mL reaction vessel. The vessel was heated to 220 ℃ for three days and then cooled to room temperature. Green crystals, with a hexagonal shape and a size of up to 2.0 mm in diameter and 0.25 mm in thickness, were isolated by washing with deionized water. The crystals were ultrasonically cleaned in water to remove impurities attached to their surfaces. For unknown reasons, different vessels contained three different types of crystals, as discussed below. The structure at room temperature was determined using single-crystal X-ray diffraction (SC-XRD) (Bruker D8 Venture). Specific heat and magnetic susceptibility measurements were conducted using physical property measurement systems (PPMS) and magnetic property measurement systems (MPMS) (Quantum Design), respectively.

Figure 1(a) shows the crystal structure of the type-I $LuCu_3$-Br, with detailed structural information provided in Table 1. This structure is the same as that of YCu_3-Br with the space group $P\bar{3}m1$ (No. 164).[20,26,27] There are two sites of Lu^{3+} ions at the center of the hexagons, with Lu2 on the kagome planes and Lu1 deviating along the c-axis. Site mixing occurs between Br^- and $(OH)^-$ at the Br sites, with a mixing ratio similar to that of YCu_3-Br.[20,28] Despite this site disorder, the kagome planes formed by the Cu^{2+} ions are not distorted. The Cu-O-Cu angle is 114.3(6)° , which is smaller than that of YCu_3-Br.[20]

Table 1. Nuclear structure parameters of the type-I sample, $LuCu_3(OH)_6Br_2[Br_{0.65}(OH)_{0.35}]$, with a space group of $P\bar{3}m1$ (No. 164): $a = b = 6.6047$ Å, $c = 6.0720$ Å, $\alpha = \beta = 90°$, $\gamma = 120°$. R: 0.0353. S: 1.354.

Atom	x	y	z	Occ.	U (Å^2)
Lu1	0	0	0.8644(3)	0.3723(13)	0.0107(4)
Lu2	0	0	1	0.255(3)	0.0107(4)
Cu1	0.5	0.5	1	1	0.0164(4)
Br1	2/3	1/3	0.6471(3)	1	0.0176(4)
Br2	0	0	0.5	0.646(17)	0.0215(13)
O1	0.1850(9)	0.3701(18)	0.8740(17)	1	0.043(3)
O2	0	0	0.5	0.354(17)	0.0215(13)

Table 2. Nuclear structure parameters of the type-Ⅱ S1 sample, $LuCu_3(OH)_6Br_2[Br_{0.33}(OH)_{0.67}]$, with a space group of $R\bar{3}$ (No. 148): $a = b = 11.4584$ Å, $c = 18.0236$ Å, $\alpha = \beta = 90°$, $\gamma = 120°$. R: 0.0259. S: 1.214.

Atom	x	y	z	Occ.	U (Å^2)
Lu1	2/3	1/3	1/3	1	0.03549(19)
Lu2	1/3	2/3	0.37728(2)	1	0.01646(13)
Cu1	1/6	1/3	1/3	1	0.0189(2)
Cu2	0.32873(5)	0.17056(5)	0.33808(3)	1	0.01902(16)
Br1	2/3	1/3	0.49364(8)	0.496(6)	0.0212(5)
Br2	0.32987(5)	0.33043(5)	0.21498(3)	1	0.02519(17)
O1	0.3351(4)	0.4990(3)	0.36496(18)	1	0.0176(6)
O2	0.4705(4)	0.1464(3)	0.29146(19)	1	0.0195(7)
O3	0	0	0.5	1	0.042(3)
O4	0.1955(3)	0.2012(3)	0.39025(18)	1	0.0182(6)
O5	2/3	1/3	0.49364(8)	0.504(6)	0.0212(5)

Table 3. Nuclear structure parameters of the type-Ⅱ S2 sample, $LuCu_3(OH)_6Br_2[Br_{0.29}(OH)_{0.71}]$, with a space group of $R\bar{3}$ (No. 148): $a = b = 11.4606$ Å, $c = 17.9904$ Å, $\alpha = \beta = 90°$, $\gamma = 120°$. R: 0.0241. S: 1.169.

Atom	x	y	z	Occ.	U (Å^2)
Lu1	2/3	1/3	0.3406(6)	0.5	0.0191(12)
Lu2	1/3	2/3	0.28975(2)	1	0.00751(11)
Cu1	1/6	1/3	1/3	1	0.00968(17)
Cu2	0.49166(4)	0.49611(4)	0.32880(3)	1	0.00960(14)
Br1	2/3	1/3	0.49349(7)	0.427(5)	0.0114(5)
Br2	0.66373(4)	0.99660(4)	0.45179(3)	1	0.01681(14)
O1	1/3	2/3	1/6	1	0.033(2)
O2	0.5008(3)	0.6647(3)	0.36569(17)	1	0.0089(5)
O3	0.3273(3)	0.4660(3)	0.27666(16)	1	0.0090(5)
O4	0.6584(3)	0.5202(3)	0.37548(17)	1	0.0099(5)
O5	2/3	1/3	0.49349(7)	0.573(5)	0.0114(5)

The structure of the type-Ⅱ $LuCu_3$-Br is similar to that of Y_3Cu_9-Cl with space group $R\bar{3}$ (No. 148),[29–31] as shown in Fig. 1(b). In this structure, the a and b lattice constants are approximately $\sqrt{3}$ times the values in the type-I sample, and the c axis is tripled. These two significantly different structures can be easily distinguished based on the diffraction patterns of the $[H,K]$ plane at $L = 1/3$ in the notation of the $P\bar{3}m1$ space group, as shown in Figs. 1(c) and 1(d), where the scattering at the $[H,K,1/3]$ positions is only allowed in the $R\bar{3}$ structure. Interestingly, two types of samples with the $R\bar{3}$ structure were found; detailed structure information is provided in Tables 2 and 3. In both samples, the directions of a and b were no longer along the nearest Cu–Cu bonds, but along the centers of the next nearest neighbor hexagons. The Cu^{2+} kagome layer is distorted, with Cu1 deviating from the symmetrical position. Notably, the c-axis deviation of Cu2 from the kagome plane is approximately 0.085 Å, which is significantly larger than that of Y_3Cu_9-Cl (≈ 0.036 Å). The six Cu–Cu bonds of the hexagon with the Lu1 ion at the center were the same, whereas the other hexagons had alternating Cu–Cu bonds. The corresponding three Cu-O-Cu angles are 109.17(15)°, 114.09(19)°, and 116.65(16)° for the type-Ⅱ S1 sample, and 109.16(16)°, 113.74(18)°, and 116.34(17)° for the type-Ⅱ S2 sample, which are systematically smaller than those in

YCu_3Cu_9-Cl,[29–31] suggesting smaller exchange couplings in type-Ⅱ $LuCu_3$-Br. The major difference between these two samples is that the Lu^{3+} ions at the Lu1 position in the type-Ⅱ S2 deviate from the centers of the hexagons by approximately 0.13 Åalong the c-axis with two randomly distributed positions, whereas those in the type-Ⅱ S1 sample remain within the planes. Note that a larger value of U ($\approx 0.03549(19)$ Å^2) at the Lu1 position was found in the type-Ⅱ S1 sample, which may indicate a tendency to occupy two separate positions, as in the type-Ⅱ S2 sample. However, the refinement program failed to provide a result if we attempted to set the Lu1 position to deviate from 1/3. We also note that although the molecular formula of the type-Ⅱ S1 sample can be written as $Lu_3Cu_9(OH)_{19}Br_8$, similar to that of Y_3Cu_9-Cl, a larger uncertainty ($R = 0.0467$) will be obtained if the Br^- and $(OH)^-$ ions are distributed in an orderly manner. Currently, we cannot clearly distinguish between these subtle structural differences.

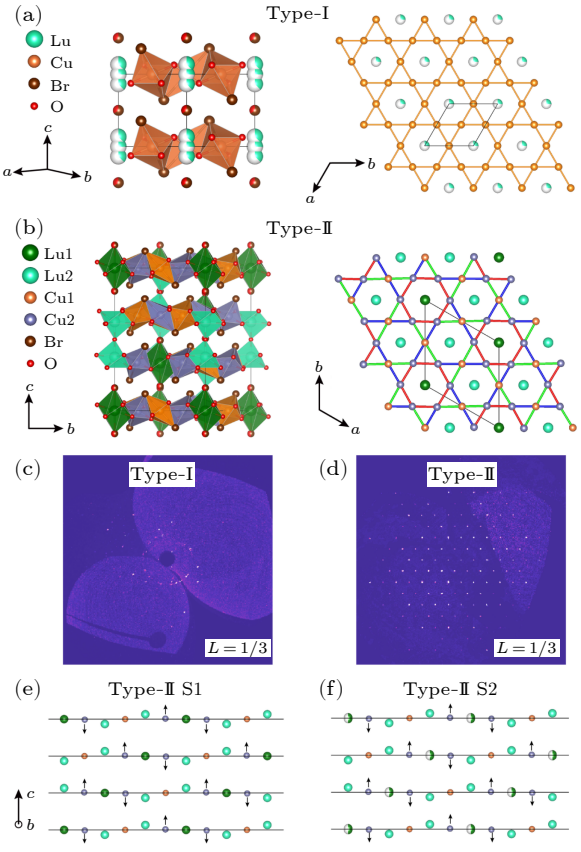

Fig. 1. (a) Crystal structure of the type-I $LuCu_3$-Br in 3D (left) and top (right) views. Hydrogen ions are not shown in any figure. (b) Crystal structure of the type-Ⅱ $LuCu_3$-Br in 3D (left) and top (right) views. (c) and (d) Diffraction patterns of the $[H, K, 1/3]$ plane for the type-I and type-Ⅱ samples, respectively, in the notation of a $P\bar{3}m1$ space group. (e) and (f) Crystal structures viewed along the b axis for type-Ⅱ S1 and S2 samples, respectively. Only Cu^{2+} and Lu^{3+} ions are shown. The arrows indicate the deviating directions of Cu ions along the c-axis.

Figure 2 shows the magnetic susceptibility and magnetization results for these samples, which exhibit no significant differences. The high-temperature susceptibilities of the samples were fitted using the Curie–Weiss function $\chi = C/(T-\Theta)+\chi_0$, where C, Θ, and χ_0 are the Curie constant, Weiss temperature, and temperature-independent background, respectively. The Weiss temperatures Θ_{ab} and Θ_c of the type-I sample, for the fields perpendicular and parallel to the c-axis, are −42 and −46 K, respectively; those for the type-Ⅱ S1 and S2 samples are the same, at approximately −50 and −60 K. We note that there is some uncertainty in these values because of the choice of the fitting temperature range and background; however, Θ of the type-I sample is systematically smaller than those of the type-Ⅱ samples. This is consistent with the field dependence of magnetization, as shown in Figs. 2(b), 2(d), and 2(f), where the slope of the type-I sample is slightly larger than those of the type-Ⅱ samples. These data also show that the ratio of the slope between $H \parallel c$ and $H \parallel ab$ is approximately 1.01 and 1.05 for the type-I and type-Ⅱ samples, respectively, suggesting that the magnetic anisotropy of all the samples is small.

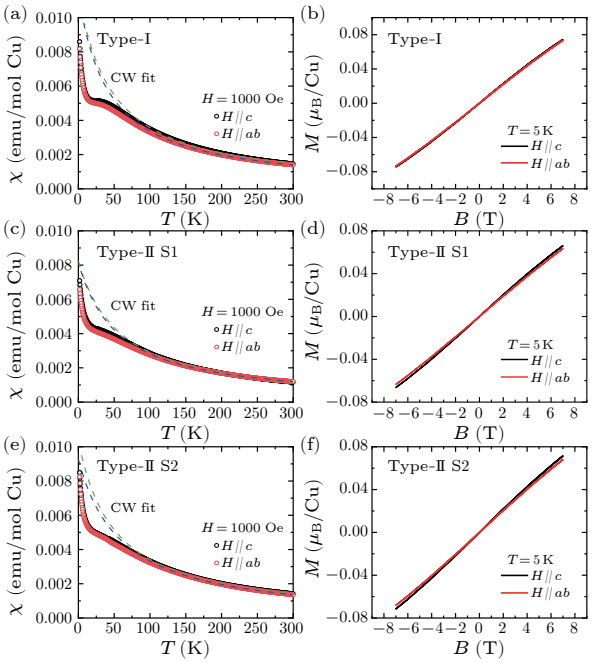

Fig. 2. (a) Temperature dependence of the magnetic susceptibility of the type-I sample. The dashed lines are the fitted results using the Curie–Weiss function as described in the text. (b) Field dependence of the magnetization of the type-I sample at 5 K. (c) and (d) Same measurements as those in (a) and (b) for the type-Ⅱ S1 sample. (e) and (f) Same measurements as those in (a) and (b) for the type-Ⅱ S2 sample.

Figure 3(a) shows the temperature dependence of the specific heat divided by the temperature, that is, C/T, for the type-I sample, where a small hump appears at $T^* \approx$ 14 K. This hump is similar to that in the C/T graph for YCu_3-Cl, which may be caused by Dzyaloshinskii–Moriya (DM) anisotropy.[34] We note that a larger hump was also observed at approximately 2.5 K. This is a shoulder-like feature of the specific heat C that has been widely observed in the KHA system.[35] The upturn below approximately 0.3 K is due to the nuclear Schottky anomaly. Below 1.5 K, another broad hump appears, which can be eas-

ily suppressed by the magnetic field, as shown in Fig. 3(b). We attributed this hump to the AFM order, the origin of which requires further study. The specific heat above 6 T shows little field dependence and exhibits a T^2 behavior, i.e., $C/T = \alpha T$ with $\alpha \approx 0.21\,\mathrm{J/mol{\cdot}K^3}$.

The temperature dependence of C/T for the type-Ⅱ S1 sample is shown in Fig. 3(c), where the hump at T^* in the specific heat of the type-I sample disappears. The low-temperature hump appears at approximately 1.8 K. Moreover, no magnetic ordering is found down to 0.15 K, as shown in Fig. 3(d). The upturn below approximately 0.3 K is due to the nuclear Schottky anomaly and can be described by AT^{-3}, where A is the fitting parameter. Thus, the data below 0.7 K can be fitted by $C/T = AT^{-3} + \alpha T^n$, where α and n are the fitting parameters. The fitted n was approximately 1.1, indicating a quadratic temperature dependence within the resolution of our data. As the field increased, the hump at approximately 1.8 K was gradually suppressed, whereas the specific heat below 1 K increased with increasing field. This results in a nonzero value of C/T at zero K, suggesting a linear temperature dependence of the specific heat, that is, $C/T = \alpha T + \gamma$. The low-temperature specific heat of the type-Ⅱ S2 sample showed a very similar behavior, as shown in Fig. 3(e). At high fields, the γ values of both samples exhibit a linear field dependence with different slopes, as shown in Fig. 3(f). Interestingly, the linear dependence of γ starts at approximately 2 T and 4 T for the S1 and S2 samples, respectively, whose origin is yet to be studied.

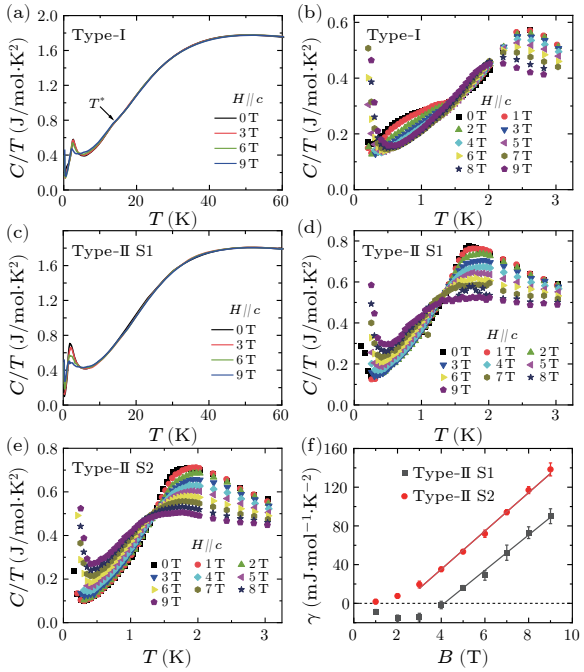

Fig. 3. (a) and (b) Temperature dependence of C/T for the type-I sample at high and low temperatures, respectively. The arrow in (a) indicates the small hump at about 14 K. (c) and (d) Temperature dependence of C/T for the type-Ⅱ S1 sample at high and low temperatures, respectively. (e) Temperature dependence of C/T for the type-Ⅱ S2 sample at low temperatures. (f) The field dependence of γ. The solid lines are fitted results using the linear function.

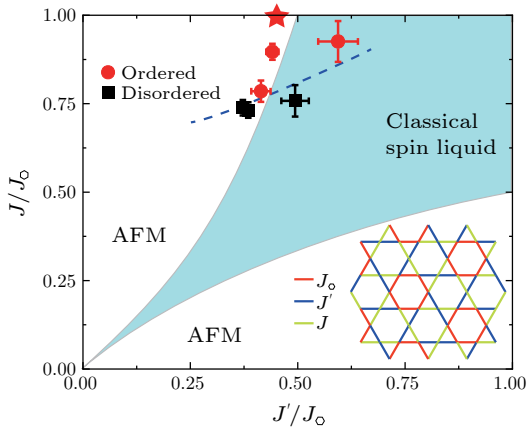

Fig. 4. Phase diagram of the $J_\bigcirc$-J-J' model from Ref. [33]. The configuration of three exchange couplings is illustrated in the inset. The red star is from Ref. [32]. The red circles and black squares are calculated results of Y_3Cu_9-Cl and $LuCu_3$-Br based on the Cu-O-Cu angles as discussed in the main text for the ordered and disordered samples, respectively. The dashed line is a guide to the eye.

Our results provide important insights into the relationship between the nuclear structure and magnetic ground states. Previous studies on the YCu_3-Br and chlorine substituted systems have shown that the magnetic order disappears in the kagome structure when the proportion of ABHs is approximately two thirds. A recent study on $LuCu_3$-Br with a kagome structure and approximately 87.4% ABHs also showed no magnetic ordering.[36] Therefore, whenever the proportion of ABHs is large, the kagome spin system becomes disordered and possibly a QSL. However, our results for the type-I sample suggest that magnetic ordering can still occur in the kagome lattice, even when the proportion of ABHs is large (approximately 74.5% ABHs for the type-I sample).

Although the ABHs are supposed to be randomly distributed in an unknown manner, they are aligned in an orderly manner in Y_3Cu_9-Cl, resulting in an enlarged unit cell with the space group $R\bar{3}$. Both magnetically ordered and disordered states have been observed in this system, with the latter potentially arising from randomness and disorder.[31] Using two new $LuCu_3$-Br samples with a $R\bar{3}$ structure, we argue that the ground states are determined by their exchange couplings. As previously shown, the spin system can be described by the $J_\bigcirc$-J-J' Heisenberg model with three different nearest exchange couplings,[32,33] as shown in Fig. 4. Although it is difficult to precisely determine these exchanges, we can estimate their values using the Cu-O-Cu angle ϕ. Various estimation methods have been proposed.[37–39] Here, we used $J \propto (\phi - 90)^3$, such that the calculated exchange couplings of Y_3Cu_9-Cl are close to those obtained by inelastic neutron scattering (the star in Fig. 4).[32] Accordingly, Fig. 4 shows the positions in the phase diagram for all the reported Y_3Cu_9-Cl[29–32] samples and type-Ⅱ $LuCu_3$-Br samples in this work. Broadly, they can be divided into two categories: magnetically ordered and disordered samples, above and below the dashed line, respectively. These roughly esti-

mated values cannot be exactly mapped onto the theoretical phase diagram, which is not exact without considering quantum effects and other interactions; however, the trend seems to hold: When the unequal exchanges in an ABH, J and J', are close, the system tends to be disordered. Therefore, the spin liquid state is most likely obtained by tuning the exchange couplings rather than randomness and disorder.

The behavior of the low-temperature specific heat in the type-Ⅱ samples is very similar to that in YCu_3-Br,[20] suggesting that their magnetic ground state is a Dirac QSL. Notably, the possible QSL state seems robust against disorder because there is significant site mixing between the Br^- and $(OH)^-$ ions at the Br1 site in the type-Ⅱ samples. The coefficients of the T^2-term α at 0 T for the type-Ⅱ S1 and S2 samples are 0.37 and 0.25 $J/mol{\cdot}K^3$, respectively. Moreover, a larger field was required to induce a linear T term in the S2 samples. Whether these differences are associated with structural differences between the two samples is worth studying further. These results suggest that the type-Ⅱ $LuCu_3$-Br samples are promising candidates for Dirac QSLs. Interestingly, because their exchange couplings are smaller than those of YCu_3-Br, a 1/9 magnetization plateau and quantum oscillations may be observed at lower fields.[22–25]

Acknowledgements. This work was supported by the National Key Research and Development Program of China (Grant Nos. 2022YFA1403400 and 2021YFA1400400) and Strategic Priority Research Program (B) of the Chinese Academy of Sciences (Grant Nos. XDB33000000 and GJTD-2020-01).

References

[1] Sachdev S 1992 *Phys. Rev. B* **45** 12377
[2] Hastings M B 2000 *Phys. Rev. B* **63** 014413
[3] Balents L, Fisher M P A, and Girvin S M 2002 *Phys. Rev. B* **65** 224412
[4] Ramirez A P 1994 *Annu. Rev. Mater. Res.* **24** 453
[5] Balents L 2010 *Nature* **464** 199
[6] Messio L, Bernu B, and Lhuillier C 2012 *Phys. Rev. Lett.* **108** 207204
[7] Norman M R 2016 *Rev. Mod. Phys.* **88** 041002
[8] Savary L and Balents L 2016 *Rep. Prog. Phys.* **80** 016502
[9] Zhou Y, Kanoda K, and Ng T K 2017 *Rev. Mod. Phys.* **89** 025003
[10] Broholm C, Cava R J, Kivelson S A *et al.* 2020 *Science* **367** eaay0668
[11] Ran Y, Hermele M, Lee P A *et al.* 2007 *Phys. Rev. Lett.* **98** 117205
[12] Hermele M, Ran Y, Lee P A *et al.* 2008 *Phys. Rev. B* **77** 224413
[13] Iqbal Y, Becca F, and Poilblanc D 2011 *Phys. Rev. B* **84** 020407
[14] Iqbal Y, Poilblanc D, and Becca F 2014 *Phys. Rev. B* **89** 020407
[15] He Y C, Zaletel M P, Oshikawa M *et al.* 2017 *Phys. Rev. X* **7** 031020
[16] Liao H J, Xie Z Y, Chen J *et al.* 2017 *Phys. Rev. Lett.* **118** 137202
[17] Geim A K and Novoselov K S 2007 *Nat. Mater.* **6** 183
[18] Hasan M Z and Kane C L 2010 *Rev. Mod. Phys.* **82** 3045
[19] Vafek O and Vishwanath A 2014 *Annu. Rev. Condens. Matter Phys.* **5** 83
[20] Zeng Z Y, Ma X Y, Wu S *et al.* 2022 *Phys. Rev. B* **105** L121109
[21] Zeng Z Y, Zhou C K, Zhou H L *et al.* 2024 *Nat. Phys.* **20** 1097
[22] Jeon S, Wulferding D, Choi Y *et al.* 2024 *Nat. Phys.* **20** 435
[23] Zheng G, Zhu Y, Chen K W *et al.* 2023 arXiv:2310.07989
[24] Suetsugu S, Asaba T, Kasahara Y *et al.* 2024 *Phys. Rev. Lett.* **132** 226701
[25] Zheng G, Zhang D, Zhu Y *et al.* 2024 arXiv:2409.05600
[26] Chen X H, Huang Y X, Pan Y *et al.* 2020 *J. Magn. Magn. Mater.* **512** 167066
[27] Liu J B, Yuan L, Li X *et al.* 2022 *Phys. Rev. B* **105** 024418
[28] Xu A N, Shen Q X, Liu B *et al.* 2024 *Phys. Rev. B* **110** 085146
[29] Puphal P, Bolte M, Sheptyakov D *et al.* 2017 *J. Mater. Chem. C.* **5** 2629
[30] Barthélemy Q, Puphal P, Zoch K M *et al.* 2019 *Phys. Rev. Mater.* **3** 074401
[31] Sun W, Arh T, Gomilšek M *et al.* 2021 *Phys. Rev. Mater.* **5** 064401
[32] Chatterjee D, Puphal P, Barthélemy Q *et al.* 2023 *Phys. Rev. B* **107** 125156
[33] Hering M, Ferrari F, Razpopov A *et al.* 2022 *npj Comput. Mater.* **8** 10
[34] Arh T, Gomilšek M, Prelovšek P *et al.* 2020 *Phys. Rev. Lett.* **125** 027203
[35] Schnack J, Schulenburg J, and Richter J 2018 *Phys. Rev. B* **98** 094423
[36] Cheng D E, Yue X Y, Zhang W J *et al.* 2024 *Phys. Rev. Mater.* **8** 114402
[37] Shimizu T, Matsumoto T, Goto A *et al.* 2003 *Phys. Rev. B* **68** 224433
[38] Rocquefelte X, Schwarz K, and Blaha P 2012 *Sci. Rep.* **2** 759
[39] Otto H H 2015 *World J. Condens. Matter. Phys.* **5** 160